Supplement to: Meltwater runoff and glacier mass balance in the high Arctic: real-time updating 1991-2022 simulations for Svalbard

Louise Steffensen Schmidt[1], Thomas V. Schuler[1], Erin Emily Thomas[2,3], and Sebastian Westermann[1]

[1]Department of Geosciences, University of Oslo, Norway
[2]Norwegian Meteorological Institute, Oslo, Norway.
[3]Current Affiliation: Fluid Dynamics and Solid Mechanics, Los Alamos National Laboratory, Los Alamos, NM, USA

Correspondence: Louise Steffensen Schmidt (l.s.schmidt@geo.uio.no)

S1 CryoGrid snow and firn physics

In this section, we describe the important components of the snow and firn scheme used in this study, focusing on the features that differ from the default CROCUS scheme in Vionnet et al. (2012) and Westermann et al. (2022).

S1.1 Albedo and short-wave penetration

The calculation of albedo and shortwave penetration is spectrally resolved into three separate bands ([0.3-0.8], [0.8-1.5], and [1.5-2.8]μm). Snow albedo mostly depends on the amount of light absorbing impurities and snow microstructure. The microstructure of the snow is represented by the optical diameter, which is determined by an empirical formulation dependent on the grain size, the snow sphericity, and the snow dendricity. The amount of light absorbing impurities is parameterised from the age of the snow. In the first spectral band ([0.3-0.8]μm), the albedo depends on both the microstructure and the amount of impurities, while at longer wavelengths it only depends on the microstructure. For further details and equations, we refer to Vionnet et al. (2012).

After calculating the spectral albedo, the amount of reflected solar radiation is calculated in each spectral bands, and the remaining radiation penetrates into the snowpack. The radiation absorption follows an exponential decay as a function of snow depth. For thin snow covers, the short-wave radiation will penetrate through the snow and interact with the underlying class. The effect of an underlying layer on the albedo is therefore taken into account in the radiation balance.

S1.2 Heat conduction

Heat transport through the snow and firn depends on both heat conduction and heat advection. The heat transport from conduction q_{hc} [$\mathrm{W\,m^{-2}}$] is calculated from Fourier's law,

$$q_{hc} = -K_s \frac{\partial T}{\partial z} \tag{S1}$$

where K_s is the thermal conductivity of snow [$\mathrm{W\,m^{-1}\,K^{-1}}$], T is the temperature [K], and z is the vertical coordinate [m]. We use a density dependent snow thermal conductivity as formulated by Yen (1981)

$$K_s = K_i \left(\frac{\rho_s}{\rho_w} \right)^{1.88} \tag{S2}$$

where ρ_w is the density of water [$\mathrm{kg\,m^{-3}}$]. The heat transfer from advection of liquid water q_{ha} [$\mathrm{W\,m^{-2}}$] is calculated as

$$q_{ha} = \rho_w c_w T q_w \tag{S3}$$

where c_w is the specific heat capacity of water [$\mathrm{J\,kg^{-1}\,K^{-1}}$] and q_w is the water flux [$\mathrm{m\,s^{-1}}$] (see Sect. **??**). The change in temperature through the subsurface is then given by

$$\rho_s c_s \frac{\partial T}{\partial t} - L_f \frac{\partial H_s}{\partial t} = -\frac{\partial q_{hc}}{\partial z} - \frac{\partial q_{ha}}{\partial z} \tag{S4}$$

where c_s is the specific heat capacity of snow [$\mathrm{J\,kg^{-1}\,K^{-1}}$], L_f is the volumetric latent heat of water freezing [$\mathrm{J\,m^{-3}}$], and H_s is the snow content [m w.e.]. Latent heat release due to freezing of water is accounted for in the second term of Eq. S4 .

S1.3 Snow and firn densification

Snowfall is added to the module with properties derived from air temperature and wind speed such as density, grain size, dendricity and sphericity. The density of new snow ρ_{new} is determined by

$$\rho_{new} = \max(\rho_{min}, a_\rho + b_\rho(T_a - T_{melt}) + c_\rho U^{0.5}) \tag{S5}$$

where ρ_{min} is the minimum density of new snow [$\mathrm{kg\,m^{-3}}$], T_a is the air temperature [k], T_{melt} is the melting temperature of snow [k], U is the windspeed [$\mathrm{m\,s^{-1}}$], and a_ρ, b_ρ, and c_ρ are constants. Following Vionnet et al. (2012), we use $a_\rho = 109$ kg m^{-3} and $b_\rho = 6$ kg m^{-3} K^{-1}. To better estimate the wind effect on density in the Arctic, we set $c_\rho = 52$ kg m$^{-7/2}$ s$^{-1/2}$ as suggested by Royer et al. (2021).

The snow undergoes metamorphism based on the internal temperature gradient, water content, and weight of overlying layers:

$$\frac{d\rho}{dt} = -\frac{\rho\sigma}{\eta} \tag{S6}$$

where ρ is the density, σ is the stress, and η is the viscosity, defined as

$$\eta = f_1 f_2 \eta_0 \frac{\rho}{c_n} \exp(a_\eta(T_{melt} - T) + b_\eta \rho). \tag{S7}$$

where f_1 and f_2 are snow-viscosity correction factors and $\eta_0 = 7.62237 \cdot 10^6$ kg s^{-1} m^{-1}, $a_\eta = 0.1\mathrm{K}^{-1}$, $b_\eta = 0.023$ m^3 kg^{-1}, and $c_\eta = 250$ kg m^{-3} are constants.

CROCUS also includes the impact of wind drift on snow grain properties and density. For each surface snow layer i, the densification from wind compaction is determined by

$$\frac{\delta \rho_i}{\delta t} = \frac{(\rho_{max} - \rho_i) W_{\text{eff}} \Gamma_{i,drift}}{\tau} \tag{S8}$$

where t is the time in hours, ρ_{max} is the maximum density impacted by wind, W_{eff} is an empirical coefficient describing the wind effect, $\Gamma_{i,drift}$ is the grain driftability, and τ is a characteristic time for snow grain change, empirically found to be 48 hours (Vionnet et al., 2012). In this study, we set $W_{\text{eff}} = 3$, as this was found to give the best estimates under Arctic conditions (Royer et al., 2021).

S2 Evaluation of forcing data

S2.1 Differences between CARRA and AROME-ARCTIC

Figure S1 and S2 show the comparison between the average AROME-ARCTIC and CARRA forcing for the overlap period from 2016-2021. The AROME-ARCTIC quantities are linearly interpolated onto the CARRA grid.

The average yearly 2m temperature over 2016-2021 (Fig. S1) is lower in most locations in AROME-ARCTIC. Over the whole domain, the yearly temperature in AROME-ARCTIC is -0.6°C colder than CARRA. The biggest difference is in NW Spitsbergen, where AROME-ARCTIC is ~ -2°C colder than CARRA.

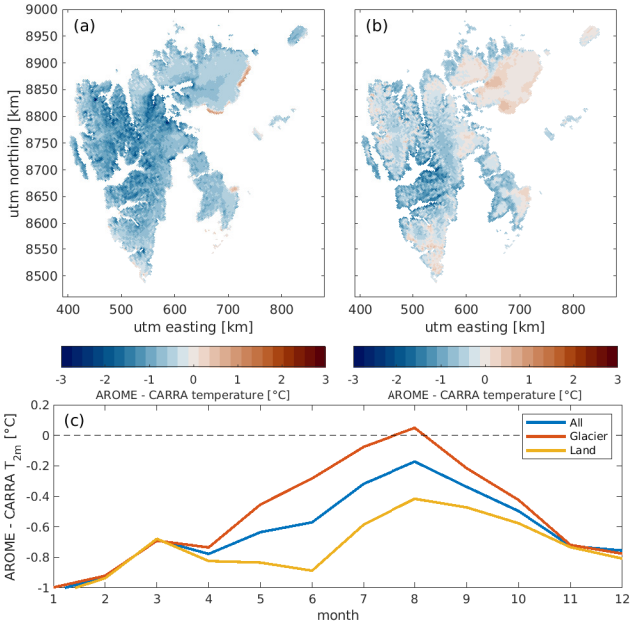

Figure S1. Seasonal Average difference between AROME-ARCTIC and CARRA 2m temperature for the a) winter months (October-April), b) summer months (May-September), and c) every month.

Figure S1 also shows the average summer and winter temperatures, in addition to the monthly mean temperatures. AROME-ARCTIC is consistently colder than CARRA during the winter months (October-April), while glacier-covered and land points show different patterns during the summer (May-September). During summer, many glacier-covered points in AROME-ARCTIC are warmer than CARRA, while the land-covered points continue to be colder. This may partly be attributed to an error in the glacier mask in AROME-ARCTIC from 2016-2018, where parts of the glacier-covered area was initiated with a too thin snow cover and thus melted completely during the summer months. Overall, AROME-ARCTIC is on average -0.8°C and -0.4°C colder than CARRA during the winter and summer, respectively. During the summer, glacier and land points are -0.2°C and -0.6°C colder in AROME-ARCTIC, respectively.

Looking at the variations in the 3-hour time series of temperature in each points, the root-mean-square deviation ranges from 1.2-2.7°C over the domain, with an average value of 1.8°C. The correlation between the two forcings is high at all points (r > 0.96).

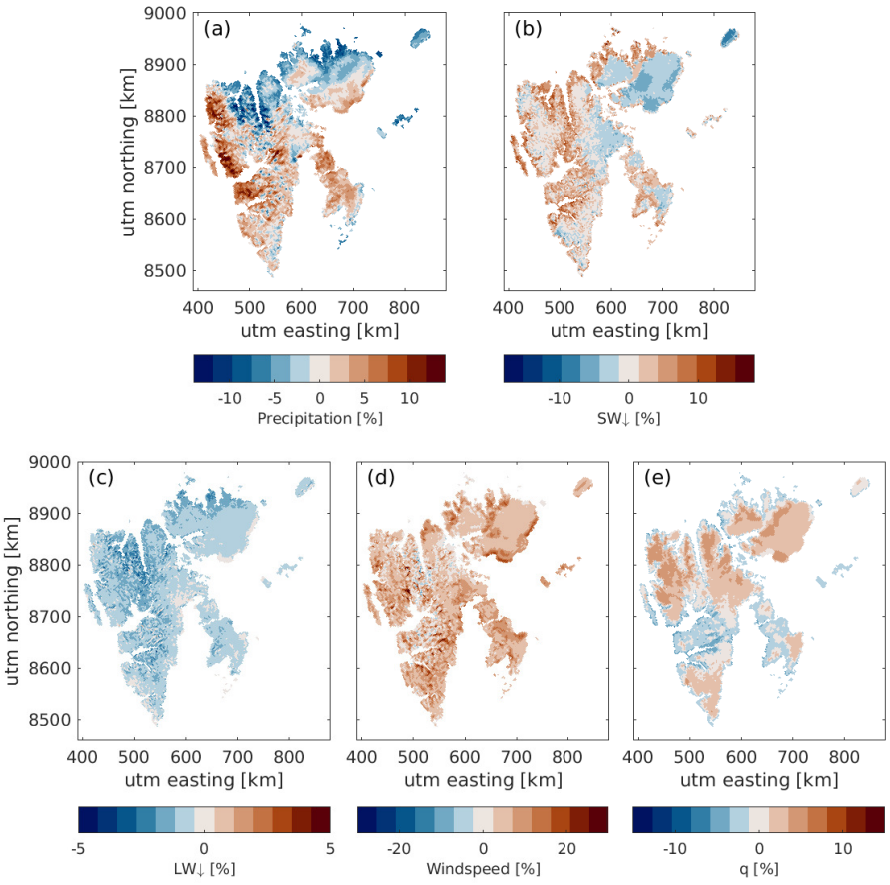

Figure S2. Average yearly percentage difference in forcing fields from AROME-ARCTIC and CARRA forcing for 2016-2021. a) precipitation, b) incoming SW, c) incoming LW, d) windspeed, e) specific humidity.

The average precipitation over Svalbard is the same for the two forcings (0.69 $\mathrm{m\,w.e.\ a^{-1}}$), but the spatial distribution differs slightly (Fig. S2a). AROME-ARCTIC predicts higher precipitation around NW Spitsbergen and Nordenskiöldland, but lower precipitation along the northern coastline. The maximum difference between the forcings is 0.15 $\mathrm{m\,w.e.\ a^{-1}}$ or 19%. The 3-hour timeseries at each point has an average root-mean-square deviation of $3.6 \cdot 10^{-3}\ \mathrm{m\,day^{-1}}$, varying between $1.9 \cdot 10^{-3} - 7.8 \cdot 10^{-3}\ \mathrm{m\,day^{-1}}$. The correlation ranges from 0.60 to 0.87, with the lowest correlations located near the coast lines and the highest correlations in high-elevation areas.

The average difference between the incoming radiation components is low overall, with values of $1.0\ \mathrm{W\,m^{-2}}$ (equivalent to 1.3%) for the incoming shortwave (Fig. S2b) and $-2.7\ \mathrm{W\,m^{-2}}$ (-1.1%) for the incoming longwave (Fig. S2c). AROME-

ARCTIC has slightly lower incoming shortwave radiation than CARRA over glacier-covered areas (-1.2 $\mathrm{W\,m^{-2}}$) and a slightly higher value over land-areas (3.3 $\mathrm{W\,m^{-2}}$), with a maximum absolute difference of 14 $\mathrm{W\,m^{-2}}$ (19%). There is generally less incoming longwave radiation in AROME-ARTIC, an indication of less cloud formation and/or clouds that are more optically thin. The largest average absolute difference is 9.9 $\mathrm{W\,m^{-2}}$ (4%).

The root-mean-square deviation in the 3-hour forcing time series ranges from 40-59 $\mathrm{W\,m^{-2}}$ for the incoming shortwave and 20-27 $\mathrm{W\,m^{-2}}$ for the incoming longwave. For both radiation components, the correlation between AROME-ARCTIC and CARRA is high (r > 0.85).

For the majority of Svalbard, the average yearly wind speeds (Fig. S2d) are larger in AROME-ARCTIC than CARRA by on average $0.36\ \mathrm{m\,s^{-1}}$ (6.2%). The root-mean-square deviation between the two forcings is on average $1.9\ \mathrm{m\,s^{-1}}$, with variations between 1.5-2.6 $\mathrm{m\,s^{-1}}$ over the domain. The correlation is generally high (r> 0.73).

Finally, the difference in specific humidity between AROME-ARCTIC and CARRA is small overall ($0.017\ \mathrm{g\,kg^{-1}}$ or 0.78%), albeit AROME-ARCTIC clearly has larger values over glaciers (0.06 $\mathrm{g\,kg^{-1}}$ or 2.6%) and lower values over land points (-0.03 $\mathrm{g\,kg^{-1}}$ or -1.2%) (Fig. S2e). The largest average absolute difference is 0.17 $\mathrm{g\,kg^{-1}}$ (6.8%). The root-mean-square deviation between AROME-ARCTIC and CARRA varies between 0.23 and 0.47 $\mathrm{g\,kg^{-1}}$, with an average of 0.32 $\mathrm{g\,kg^{-1}}$. The correlation is high over the whole Svalbard land area (r > 0.95).

S2.2 CARRA evaluation (1991-2021)

Table S1 compares the CARRA forcing against observations from automatic weather stations. For the glacier stations, the albedo and outgoing longwave radiation simulated by CryoGrid is also evaluated. The MET Norway stations are given as an average over all 20 stations - the values for individual stations are shown in the in supplement Table S3. The MET Norway stations have been assimilated into the CARRA product, and it is therefore not surprisingly that there is a good agreement between the two. The largest differences in temperature is found for the Sveagruve II station ($\Delta T = -1.8^{\circ}\mathrm{C}$), but for most of the MET Norway stations the mean temperature difference is below $1^{\circ}\mathrm{C}$. The largest different in relative humidity and wind speed is found at Kvitøya ($\Delta RH = 6.4\%$) and Pyramiden ($\Delta WS = -1.9\ \mathrm{m\,s^{-1}}$), respectively.

The 2m temperature, relative humidity, and wind speed at the glacier stations, which were not assimilated into the CARRA product, are generally well represented. The exception is at the Etonbreen AWS, where CARRA has a cold bias. This can, however, partly be attributed to a warm bias in the AWS observations over time at this station due to an error with the temperature sensor.

Figure S3 shows the monthly mean observed temperature and the monthly mean temperature difference. At Etonbreen, there is a consistent cold bias, while at Nordenskiöldbreen there is a consistent warm bias. At the other glacier stations, CARRA generally has only a low bias over the summer but a warm bias in the winter months. At the MET Norway stations, the monthly mean bias is small overall, but with variations of up to $\pm 2^{\circ}\mathrm{C}$ for individual stations.

The radiation balance is only measured at the stations situated on glaciers. The incoming longwave and shortwave radiation in CARRA generally fits well with the observations, albeit with a small negative bias in the longwave radiation for most of the stations. The albedo, calculated in CryoGrid, is underestimated overall at all stations, which can mostly be attributed to an

Table S1. Evaluation of modelled results against observations from automatic weathers stations on Svalbard from 1991-2021. The MET Norway column is a weighted average for all stations operated in Svalbard by the Norwegian Meteorological Office. For each station and quantity, the annual mean of the observations, bias (Δ) and root mean squared error (RMSE) is given. The bias is calculated as the simulations - observations.

Location	type	T [K]	RH [%]	WS [$\mathrm{m\,s^{-1}}$]	SW$\downarrow$ [$\mathrm{W\,m^{-2}}$]	LW$\downarrow$ [$\mathrm{W\,m^{-2}}$]	albedo	LW$\uparrow$ [$\mathrm{W\,m^{-2}}$]
MET Norway	AWS mean	269	80	5.7	–	–	–	–
(20 stations)	Δ	0.12	1.6	0.34	–	–	–	–
	rmse	1.3	8.9	1.9	–	–	–	–
Etonbreen	AWS mean	265	90	5.0	94	257	0.8	276
	Δ	-1.9	3.0	-0.78	0.43	-23	-0.09	-12
	rmse	3.2	7.0	2.2	32	35	0.15	22
Kongsvegen	AWS mean	267	83	4.3	128	262	0.8	287
	Δ	0.3	6.2	1.5	-9.0	19	-0.06	-5.3
	rmse	1.7	17	2.1	40	29	0.14	10
Nordenskiöld-	AWS mean	266	85	4.6	104	257	0.7	282
breen	Δ	1.6	-5.7	1.8	-0.8	-20	-0.06	-1.6
	rmse	2.0	10	2.9	36	28	0.17	7.2
Ulvebreen	AWS mean	268	87	5.1	83	272	0.7	296
	Δ	-0.5	1.2	0.9	3.4	-28	-0.003	-14
	rmse	1.1	6.6	1.9	35	33	0.14	16
Vestfonna	AWS mean	263	89	6.0	88	253	0.8	270
	Δ	0.72	0.73	0.09	8.8	-24	-0.05	-2.3
	rmse	2.6	7.7	3.3	48	40	0.11	14

underestimation of the albedo during the winter season. The outgoing longwave radiation, also calculated in CryoGrid, shows a low bias and root-mean-square error, albeit always with a negative bias.

S2.3 Forcing evaluation of CARRA and AROME-ARCTIC: 2016-2021

Table S2 shows the comparison of the CARRA and AROME-ARCTIC forcing with observations from automatic weather stations in the overlap period from 2016-2021. For the glacier stations, the albedo and outgoing longwave radiation simulated by CryoGrid is also evaluated. For this period, observations from 4 stations on glaciers and 17 stations on non-glaciated land operated by MET NORWAY are available. Not all observations span the whole period, see Supplement Table S3.

Since the MET Norway stations were assimilated into both products, we expect a good agreement between the observations from these stations and both forcing products. In AROME-ARCTIC, the temperatures are generally lower and the windspeeds slightly higher, but both forcings generally fit well with observations. The comparison for each weather stations is shown

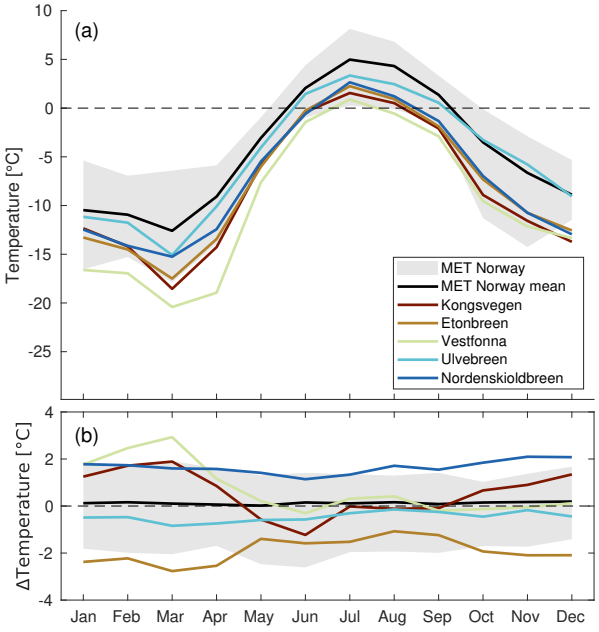

Figure S3. (a) Average monthly mean 2m temperatures for available AWS from 1991-2020, (b) average monthly mean difference between simulations and observations of the 2m temperature ($\Delta T = T_{model} - T_{AWS}$).

in supplement Table S4. The difference in temperature between CARRA and AROME-ARCTIC at the station locations is between 0.1-1.6°C, with the highest deviation at Barentsburg.

For the glacier stations, the simulations and observations are almost equal for the two forcings. However, there are some significant differences in terms of the 2m temperature, where AROME-ARCTIC generally has a larger bias and root-mean-square-error than CARRA. The opposite is true for Nordenskïoldbreen, where there is a significant warm bias in the CARRA simulations. Overall, the difference in average temperature at the station locations is 0.1-0.9°C between AROME-ARCTIC and CARRA.

The components of the radiation balance is generally similar in CARRA and AROME-ARCTIC, and both fit well with the observations, albeit with a slight underestimation in the incoming radiation.

Table S2. Evaluation of modelled results using CARRA / AROME-ARCTIC forcing against observations from automatic weathers stations on Svalbard from 2016-2021. The MET Norway column is a weighted average for all stations operated in Svalbard by the Norwegian Meteorological Office. For each station and quantity, the annual mean of the observations, bias (Δ) and root mean squared error (RMSE) is given. The bias is calculated as the simulations - observations.

Location	type	T [K]	RH [%]	WS [$\mathrm{m\,s^{-1}}$]	SW$\downarrow$ [$\mathrm{W\,m^{-2}}$]	LW$\downarrow$ [$\mathrm{W\,m^{-2}}$]	albedo	LW$\uparrow$ [$\mathrm{W\,m^{-2}}$]
MET Norway	AWS mean	270	80	5.7	–	–	–	–
(17 stations)	Δ	0.2 / -0.7	1.6 / 2.2	0.3 / 0.6	–	–	–	–
	rmse	0.9 / 1.8	6.6 / 7.4	1.8 / 2.0	–	–	–	–
Etonbreen	AWS mean	265	90	5.0	94	257	0.78	276
	Δ	-0.28 / -0.38	2.6 / 0.16	-1.0 / -0.37	0.12 / -5.7	-30 / -34	-0.06 / -0.08	-20 / -20
	rmse	2.0 / 2.8	6.9 / 6.0	2.5 / 2.6	32 / 36	40 / 48	0.15 / 0.14	28 / 30
Kongsvegen	AWS mean	268	87	4.2	117	277	0.74	298
	Δ	0.4 / 1.2	-1.5 / 4.5	1.6 / 2.1	-8.0 / -4.0	-26 / -28	-0.03 / -0.06	-12 / -12
	rmse	1.9 / 3.3	6.8 / 7.4	2.4 / 2.8	36 / 34	31 / 35	0.16 / 0.14	14 / 15
Nordenskiöld-	AWS mean	266	85	4.6	104	257	0.68	282
breen	Δ	1.8 / 0.87	-6.5 / -4.3	1.7 / 1.6	-4.4 / -6.3	-21 / -24	-0.08 / -0.08	-3.1 / -6.2
	rmse	2.1 / 1.7	11 / 11	2.8 / 2.9	37 / 39	28 / 31	0.14 / 0.15	6.9 / 9.1
Ulvebreen	AWS mean	268	87	5.1	84	272	0.66	296
	Δ	-0.47 / -0.89	1.5 / 0.62	0.90 / 1.2	3.8 / 2.6	-28 / -30	-0.01 / 0.00	-14 / -16
	rmse	1.1 / 1.7	6.5 / 8.2	1.9 / 2.2	36 / 35	33 / 36	0.14 / 0.16	16 / 18

S3 Automatic Weather Station Comparison

The comparison between CARRA reanalysis and automatic weather stations operated by the Norwegian Meteorological Office is shown in Table S3 and S4. These stations have been assimilated into the CARRA product, and the differences are therefore expected to be small.

Table S3. Evaluation of CARRA reanalysis simulations (1991-2021) against observations from automatic weathers stations on Svalbard operated by the Norwegian Meteorological Office. Differences (Δ) are calculated as the simulation - observation. The operational time period is written underneath each station name.

Station name	**Type**	**T [K]**	**RH [%]**	**WS [$\mathrm{m\,s^{-1}}$]**	**Station name**	**Type**	**T [K]**	**RH [%]**	**WS [$\mathrm{m\,s^{-1}}$]**
Edgeøya	Δ	-0.33	1.3	-0.06	Svarttangen	Δ	0.09	-	-
(1992 –)	rmse	1.5	5.9	1.5	(1904 – 2012)	rmse	1.6	-	-
Kongsøya	Δ	0.02	1.4	-0.76	Sørkappøya	Δ	0.61	0.03	-0.27
(2010 –)	rmse	0.91	12	1.4	(1908 –)	rmse	0.91	4.8	1.8
Hornsund	Δ	0.27	4.4	1.5	Sveagruva	Δ	1.2	-1.9	0.48
(1985 –)	rmse	1.1	8.4	2.3	(1978 –)	rmse	2.1	8.8	2.0
Sveagruva II	Δ	-1.8	-	1.1	Akseløya	Δ	0.67	1.3	0.49
(2016 – 2019)	rmse	1.9	-	2.6	(1898 –)	rmse	1.2	5.3	1.6
Isfjord Radio	Δ	0.15	-0.40	-0.45	Barentsburg	Δ	-0.02	-0.71	1.8
(1934 –)	rmse	0.66	7.7	1.8	(2014 – 2016)	rmse	0.58	5.7	2.8
S. Lufthavn	Δ	-0.37	4.6	0.75	Platåberget III	Δ	0.94	0.94	0.72
(1964 –)	rmse	0.92	9.0	2.2	(2018 –)	rmse	1.5	6.8	1.7
Adventdalen	Δ	0.5	-3.0	-0.85	Pyramiden	Δ	-0.5	5.7	1.9
(2016 –)	rmse	1.1	8.9	1.7	(2012 –)	rmse	0.90	10	3.2
Ny-Ålesund	Δ	0.60	3.6	0.52	A. Brøggerbreen	Δ	-1.2	-	-
(1974 –)	rmse	0.95	8.4	1.8	(1994 – 1995)	rmse	1.9	-	-
Verlegenhuken	Δ	0.17	1.1	-0.45	Crozierpynter	Δ	0.29	-	-
(1997 –)	rmse	1.27	6.6	1.6	(1899 – 2012)	rmse	1.6	-	-
Karl XII-Øya	Δ	0.90	0.71	0.38	Kvitøya	Δ	-0.13	6.4	-0.93
(2000 –)	rmse	2.4	6.0	1.4	(1986 –)	rmse	0.75	28	2.0

Table S4 shows the comparison between AROME-ARCTIC forecasts and AWSs from 2016-2021 as well as the CARRA comparison for the same period.

Table S4. Evaluation of CARRA / AROME-ARCTIC forcings against observations from automatic weathers stations on Svalbard operated by the Norwegian Meteorological Office from 2016-2021. For each station and quantity, the bias (Δ) and root mean squared error (RMSE) is given. The bias is calculated as the simulations - observations.

Station name	**Type**	**T [K]**	**RH [%]**	**WS [$\mathrm{m\,s^{-1}}$]**	**Station name**	**Type**	**T [K]**	**RH [%]**	**WS [$\mathrm{m\,s^{-1}}$]**
Edgeøya	Δ	-0.1 / -0.7	0.8 / -1.3	-0.2 / 0.3	Kongsøya	Δ	0.0 / -0.6	1 / -1.6	-0.8 / -0.2
(1992 –)	rmse	0.7 / 1.7	5.4 / 5.5	1.1 / 1.3	(2010 –)	rmse	0.6 / 1.7	6.3 / 5.6	1.4 / 1.2
Sørkappøya	Δ	0.6 / 0.4	0 / -1.6	-0.4 / -0.1	Hornsund	Δ	0.2 / -0.2	4.3 / 4.2	1.5 / 1.7
(1908 –)	rmse	0.8 / 1.2	4.2 / 4.9	1.4 / 1.5	(1985 –)	rmse	0.6 / 1.1	8.1 / 8	2.2 / 2.6
Sveagruva	Δ	1.3 / 0.4	-0.3 / 0.8	0.3 / 0.7	Sveagruva II	Δ	-1.8 / -3.0	– / –	1.1 / 1.4
(1978 –)	rmse	1.9 / 2.4	6.9 / 7.2	1.7 / 1.9	(2016 – 2019)	rmse	1.9 / 3.5	– / –	2.6 / 3.2
Akseløya	Δ	0.8 / -0.2	1.6 / 2.5	0.2 / 0.4	Isfjord Radio	Δ	0.2 / -0.6	-0.5 / 0.3	-0.5 / -0.1
(1898 –)	rmse	1.3 / 1.9	5.4 / 6.4	1.6 / 1.8	(1934 –)	rmse	0.6 / 1.3	8.2 / 8.7	1.7 / 1.8
Barentsburg	Δ	0.0 / -1.5	1.3 / 5.5	1.5 / 1.9	S. Lufthavn	Δ	-0.4 / -2	4.4 / 9.6	0.2 / 0.3
(2014 – 2016)	rmse	0.6 / 1.9	4 / 7.6	2.4 / 2.8 8	(1964 –)	rmse	0.7 / 2.4	7.8 / 11.7	1.6 / 1.8
Platåberget III	Δ	0.9 / -0.2	0.9 / 2.4	0.7 / 0.9	Adventdalen	Δ	0.5 / -0.8	-3 / 0.7	-0.9 / -0.3
(2018 –)	rmse	1.5 / 1.2	6.8 / 7	1.7 / 1.8	(2016 –)	rmse	1.1 / 1.9	8.9 / 8.1	1.7 / 1.7
Pyramiden	Δ	-0.5 / -1.6	6.1 / 8.7	2 / 2.3	Ny-Ålesund	Δ	0.5 / -0.8	4.2 / 7.9	0.5 / 1.1
(2012 –)	rmse	0.9 / 2.2	9.9 / 11.9	3.4 / 3.7	(1974 –)	rmse	0.7 / 1.6	6.8 / 10.9	1.6 / 2.2
Verlegenhuken	Δ	0.3 / -0.4	1.0 / -0.4	-0.4 / 0.0	Karl XII-Øya	Δ	0.3 / -0.2	1.7 / -0.6	0.3 / 0.4
(1997 –)	rmse	0.6 / 1.5	6 / 5.8	1.4 / 1.6	(2000 –)	rmse	0.7 / 1.7	5 / 3.8	1.1 / 1.3
Kvitøya	Δ	-0.1 / -0.2	2.6 / -1.6	-0.8 / -0.6					
(1986 –)	rmse	0.7 / 1.7	6.5 / 5.8	2.0 / 2.0					

References

Royer, A., Picard, G., Vargel, C., Langlois, A., Gouttevin, I., and Dumont, M.: Improved Simulation of Arctic Circumpolar Land Area Snow Properties and Soil Temperatures, Frontiers in Earth Science, 9, 515, https://doi.org/10.3389/feart.2021.685140, 2021.

Vionnet, V., Brun, E., Morin, S., Boone, A., Faroux, S., Le Moigne, P., Martin, E., and Willemet, J. M.: The detailed snowpack scheme Crocus and its implementation in SURFEX v7.2, Geoscientific Model Development, 5, 773–791, https://doi.org/10.5194/gmd-5-773-2012, 2012.

Westermann, S., Ingeman-Nielsen, T., Scheer, J., Aalstad, K., Aga, J., Chaudhary, N., Etzelmüller, B., Filhol, S., Kääb, A., Renette, C., Schmidt, L. S., Schuler, T. V., Zweigel, R. B., Martin, L., Morard, S., Ben-Asher, M., Angelopoulos, M., Boike, J., Groenke, B., Miesner, F., Nitzbon, J., Overduin, P., Stuenzi, S. M., and Langer, M.: The CryoGrid community model (version 1.0)-a multi-physics toolbox for climate-driven simulations in the terrestrial cryosphere, Geoscientific Model Development Discussions, https://doi.org/10.5194/gmd-2022-127, 2022.

Yen, Y.-C.: Review of Thermal Properties of Snow, Ice and Sea Ice,, 1981.